Journal of Molecular Graphics and Modelling 29 (2011) 1047–1055

Contents lists available at ScienceDirect

Journal of Molecular Graphics and Modelling

journal homepage: www.elsevier.com/locate/JMGM

The effect of electrostatics on factor H function and related pathologies

Chris A. Kieslich, Homero Vazquez, Gabrielle N. Goodman, Aliana López de Victoria, Dimitrios Morikis *

Department of Bioengineering, University of California, Riverside, CA 92521, United States

ARTICLE INFO

Article history:
Received 8 January 2011
Received in revised form 26 April 2011
Accepted 28 April 2011
Available online 6 May 2011

Keywords:
Complement system
Factor H
C3b
Poisson–Boltzmann electrostatics
Electrostatic clustering

ABSTRACT

Factor H (FH) contributes to the regulation of the complement system by binding to polyanionic surfaces and the proteins C3b/C3c/C3d. This implicates charge and electrostatic interactions in recognition and binding of FH. Despite the large amount of experimental and pathology data the exact mechanism at molecular level is not yet known. We have implemented a computational framework for comparative analysis of the charge and electrostatic diversity of FH modules and C3b domains to identify electrostatic hotspots and predict potential binding sites. Our electrostatic potential clustering analysis shows that charge distributions and electrostatic potential distributions are more useful in understanding C3b–FH interactions than net charges alone. We present a model of non-specific electrostatic interactions of FH with polyanion-rich surfaces and specific interactions with C3b, using our computational data and existing experimental data. We discuss the electrostatic contributions to the formation of the C3b–FH complex and the competition between FH and Factor Bb (Bb) for binding to C3b. We also discuss the significance of mutations of charged amino acids in the pathobiology of FH-mediated disease, such as age-related macular degeneration, atypical hemolytic uremic syndrome, and dense deposit disease. Our data can be used to guide future experimental studies.

1. Introduction

Factor H (FH) is a regulator of the complement system [1–3] that has been implicated in a variety of diseases, such as age related macular degeneration (AMD) [4–8], atypical hemolytic uremic syndrome (aHUS) [9–12], and dense deposit disease (DDD, a.k.a. membranoproliferative glomerulonephritis Type II) [9,13]. The complement system is part of innate immunity and a link between innate and adaptive immunities, whose function is tightly regulated to avoid immune attack against own tissues. FH is an essential regulator of the complement system whose absence results in breaking down the prevention of complement attack against self-tissues [1,2]. FH functions by binding to complement protein fragment C3b and acting as cofactor to serine protease Factor I (FI), which cleaves and inactivates C3b. When C3b is bound covalently to pathogen surfaces, it is amenable to binding by Factor B (FB) which is subsequently activated and forms the convertase enzyme complex C3b–Bb, where Bb is a fragment of FB. The convertase is responsible for amplified cleavage of C3 molecules and generation of additional C3b fragments that bind (opsonize) pathogen surfaces. A structural biology view of the C3 function has recently been presented [14–16].

The essence of FH regulation of the complement system depends on the charge composition of the surfaces it is capable of binding, as well as on competition with FB for binding to C3b [2]. FH binds with higher affinity to C3b than FB on host cell surfaces that are rich in polyanions, such as sialic acid and glycosaminoglycans (GAGs). On the contrary, FB binds with higher affinity to C3b than FH on pathogen surfaces that lack polyanion coating [2]. The capability of FH to interact with polyanions implicates charge in its function and renders the study of the electrostatic properties of FH necessary to understand its function.

Charge plays a role in FH's association to disease through specific amino acids or groups of amino acids that form surface hotspots. Mutations of ionizable amino acids are associated with disease. FH is implicated in AMD through a single nucleotide polymorphism (SNP) that involves a tyrosine/histidine mutation [4,6–8]. This SNP genetically predisposes part of the population to AMD. Polyanion-binding sites in FH have also been implicated in AMD and in aHUS (reviewed in [17,18]). FH is implicated in DDD through a lysine deletion [19].

FH has a chain-like structure consisting of 20 modules. These modules have the complement control protein (CCP) module topology and are called CCP modules [20]. They resemble compact ellipsoids which are connected with short and flexible loops. There are many high-resolution structures of FH CCP modules and one

Abbreviations: FH, Factor H; C3, complement system protein C3; C3b, the b-fragment of C3; CCP, complement control protein; MG, macroglobulin (referring to the α2-MG family); FB, Factor B; Bb, the b-fragment of FB; FI, Factor I; GAG, glycosaminoglycan; SNP, single nucleotide polymorphism; MCP, membrane cofactor protein; CRP, C-reactive protein; AMD, age related macular degeneration; aHUS, atypical hemolytic uremic syndrome; DDD, dense deposit disease; PDB, protein data bank.

* Corresponding author. Tel.: +1 951 827 2696.
E-mail address: dmorikis@engr.ucr.edu (D. Morikis).

1093-3263/$ – see front matter © 2011 Elsevier Inc. All rights reserved.
doi:10.1016/j.jmgm.2011.04.010

low-resolution structure of whole FH, which suggests a folded back topology that brings together the N- and C-termini [21]. In addition, the structure of the complex between the four N-terminal CCP domains of FH and C3b is available and provides the first insight on the specifics of the interaction [22]. Each FH CCP module is made of 51–62 amino acids and has a core stabilized by two disulfide bridges. Each loop is made of 3–8 amino acids. Despite similar structures and stabilities of FH CCP modules, there is a wide diversity in physicochemical properties, and most importantly in charge composition. The basic hypothesis of our study is that the charge (and electrostatic) diversity of CCP modules renders FH its binding properties to C3b and polyanion-coated surfaces. C3b is also a modular protein consisting of 8 macroglobulin (MG) domains and 5 other domains and linkers [22,23]. Despite their similar structures, the MG domains of C3b also have charge (and electrostatic) diversity.

In a recent review [1], the interactions of FH and their roles in complement regulation and disease have been discussed. However, the importance of charge and electrostatic interactions was not emphasized. Therefore, the goal of our study is to perform a comparative electrostatic analysis of all 20 CCP modules of FH and all 8 MG domains of C3b to identify electrostatic hotspots and predict potential binding sites. We also performed binding analysis of the structure of the FH(CCP1–4)–C3b and C3b–Bb complexes to gain insight on the C3b binding mechanism for competing proteins FH and Bb. The method we use is theoretical and is based on the calculation of electrostatic potentials using the Poisson–Boltzmann equation [24]. We have previously applied similar protocols in other proteins that contain CCPs and whose function is driven by electrostatic interactions, as evidenced by experimental data [25–31]. This is an atomic resolution study in which three-dimensional structures of the 20 CCP modules are needed. The basis of our study is the use of a clustering method to classify similarities or dissimilarities of the spatial distributions of electrostatic potentials of the various CCP modules of FH. We place special emphasis on CCP modules that are known from experimental data to bind to C3b and polyanion-coated surfaces, such as GAGs and sialic acid found in human cells and tissues. We also discuss those CCP modules that are implicated directly to disease. For example, the SNP and polyanion-binding hotspot implicated in AMD are located in CCP7. A polyanion-binding hotspot implicated in aHUS is in CCP20. A loss of charge mutation implicated in DDD is in CCP4. Finally, we make binding predictions for CCP modules of unknown function.

2. Materials and methods

2.1. Homology modeling of FH CCPs

Our atomic-level calculations are possible when three-dimensional structures are known at high resolution. FH has been the focus of several structural biology studies, from which several crystallographic or NMR structures for CCP modules have been determined. Currently the structures of 14 CCP modules are available, and in most cases multiple structures exist for single, double, triple, or quadruple modules (Supplementary Table S6). Modules with experimentally determined structures are: CCP1–8, 12, 13, 15, 16, and 19–20. Therefore, our initial step was the examination of all available CCP structures to (i) select those that are more suitable for our calculations and (ii) select those that are suitable to be used as templates to generate homology models for the 6 CCPs without experimentally determined structures. Our criteria for (i) were quality (resolution), completeness of the structure with maximum amount of secondary structure, and lack of selenomethionine (MSE) amino acids. MSEs are non-physiological amino acids used in crystallographic studies to solve the phases of the diffraction patterns, for which we do not have parametrization for electrostatic calculations. Supplementary Tables S7 and S8 provide a list of the experimentally derived structures used and reasoning. Our criteria for (ii) were quality of sequence alignment and percent identity. To generate homology models for CCP9–11, 14, 17, and 18 we first obtained the amino acid sequences from the SMART database [32] and subsequently we used sequence alignments with the CCP modules of known structure. All CCP domains are characterized by four conserved cysteine residues, which form two disulfide bonds (I to III and II to IV) stabilizing these relatively small domains [20]. Here we have defined the CCP domain as the residues falling between and including the first and fourth cysteines, and have removed additional amino acids that form flexible loops connecting the many CCP domains in a chain like structure. In addition to the four cysteine residues, there also exists a conserved tryptophan between the third and fourth cysteines that was taken into consideration when performing sequence alignments in the following steps. Amino acid sequence alignment scores were produced for all possible target-template pairs using the ClustalW server where default parameters were applied [33]. The templates that produced alignments with the highest percent identity score, while still providing proper alignment of the four cysteines and a conserved tryptophan close to the C-terminus were chosen. The CCP module sequences and template structures, as listed in Supplementary Tables S7 and S8 were imported into the Automodel module of the homology modeling package Modeller 9v5 [34]. After generation, each model was visualized using Deep View [35] and inspected for van der Waals clashes, secondary structure quality, and disulfide bond correctness. The complete set of structures for all 20 FH CCP modules was superimposed using Deep View for comparison. Superimposition was based on C^{α}-atoms using CCP16 as reference, because CCP16 contained the highest quality secondary structure. The coordinates of each CCP module were saved in the orientation of the superimposition. This was necessary to assure that all CCP modules had the same center and coordinate fit in the box used in subsequent Poisson–Boltzmann calculations.

2.2. Electrostatic calculations

Electrostatic potential calculations were performed using the Adaptive Poisson–Boltzmann Solver (APBS) [24], which utilizes a grid-based method to solve the linearized Poisson–Boltzmann equation. Prior to electrostatic potential calculations, partial charges and atomic radii were assigned, assuming model protonation states at pH 7, using the software PDB2PQR [36] and the PARSE force field [37]. Model pK_a values are as in [31]. A dielectric coefficient of 2 was used for the protein whereas a dielectric coefficient of 78.5 was used for the solvent. Two sets of calculations were carried out at ionic strengths corresponding to 0 mM and 150 mM concentrations, assuming +1/−1 charges for the counterions. The dielectric surface was defined using a sphere with probe radius of 1.4 Å and selecting the contact surface, whereas the ion accessibility surface was defined using a sphere with probe radius of 2.0 Å. Since the amount of screening differs between the two ionic strength parameters, the physical dimensions of the box used for each set of calculations was set to different values to ensure that the largest magnitude values were captured, while still providing maximum resolution. The grid size was $129 \times 129 \times 129$ points. A box size of 110 Å × 110 Å × 110 Å was used for the calculations corresponding to 0 mM ionic strength, whereas a box size of 60 Å × 60 Å × 60 Å was used for the calculations corresponding to 150 mM ionic strength. All CCP modules were centered on CCP16 in electrostatic potential calculations. The spatial distributions of electrostatic potential were visualized and plotted in the form of isopotential contours using the molecular graphics program Chimera [38].

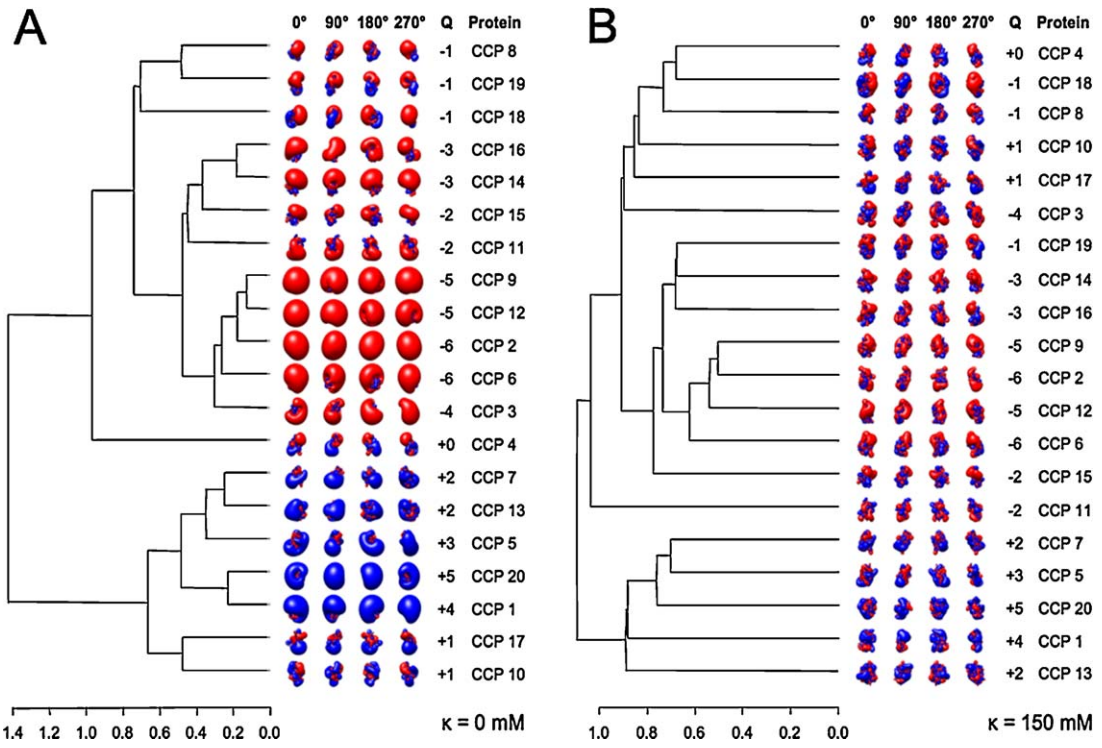

Fig. 1. Clustering diagram of the 20 CCP modules of FH according to the spatial distributions of their electrostatic potentials. Calculations of electrostatic potentials were performed using ionic strengths corresponding to 0 mM (A) and 150 mM (B) counterion concentration. Isopotential contours are plotted at $\pm 1 k_B T/e$, with blue and red corresponding to positive and negative electrostatic potential, respectively. Four orientations are shown corresponding to rotations about the vertical axis, as indicated. The net charge, *Q*, of each module is marked in the figure. (For interpretation of the references to color in this figure legend, the reader is referred to the web version of the article.)

2.3. Electrostatic clustering of FH CCPs

After calculating the electrostatic potentials, the final step was the clustering of spatial distributions of electrostatic potentials of the 20 FH CCP modules. A distance matrix was generated based on an electrostatic similarity distance (ESD). An ESD is a measure of the amount of dissimilarity between the spatial distributions of electrostatic potential for two homologous proteins and has been used previously in different protein clustering studies [39–46]. The ESD used in this study is equivalent to an average difference, and was calculated by taking the average of the normalized error between all corresponding grid points according to [40–42]

$$ESD_{A,B} = \frac{1}{N}\sum_{i,j,k}\frac{\left|\phi_A(i,j,k) - \phi_B(i,j,k)\right|}{\max\left(\left|\phi_A(i,j,k)\right|, \left|\phi_B(i,j,k)\right|\right)}$$

where $ESD_{A,B}$ is the similarity between proteins *A* and *B*, *N* is the number of grid points, and $\phi_A(i,j,k)$ and $\phi_B(i,j,k)$ refer to the electrostatic potentials of proteins *A* and *B*, respectively, at identical grid points (i,j,k). The summation is over all grid points. According to this scheme, ESD can assume values between 0 and 2, where an ESD value of 0 indicates two proteins (CCP modules here) with identical spatial distributions of electrostatic potential, while an ESD value of 2 indicates opposite potentials. The distance matrix was produced by calculating the ESD between every CCP module pair, resulting in a 20×20 array. Distance matrix generation and hierarchal clustering using average linkage was performed using in-house R scripts that utilize functions of the R-base package [47]. The clustering results are presented as dendrograms using the R plot functions.

2.4. Electrostatic clustering of C3b MG domains

Clustering was also performed for the C3b MG domains using a similar procedure. The C3b structure with PDB Code 2I07 was used [22]. Since the MG domains exhibit more structural and sequence variability than the FH CCPs, a more elaborate alignment procedure was required. The "Match Maker" module of Chimera [38] was utilized in this instance, since it includes a secondary structure score with a variable weight that provided optimal coordinate superposition. The MG domains were aligned to MG2 since this provided the best alignment. The grid size used for the MG domain calculations was $129 \times 129 \times 129$ points. A box size of 135 Å × 140 Å × 130 Å was used for the calculations corresponding to 0 mM ionic strength, whereas a box size of 65 Å × 85 Å × 60 Å was used for the calculations corresponding to 150 mM ionic strength. All CCP modules were centered on MG2 in electrostatic potential calculations.

3. Results and discussion

3.1. Rationale

The 20 CCP modules of FH are structurally homologous, but have diverse sequences and physicochemical properties. Because of the striking charge diversity among individual FH CCP modules, we initiated this structural bioinformatics study to examine the electrostatic properties of CCP modules in terms of net charge, spatial distributions of charge and electrostatic potentials. Our goal is to classify CCP modules according to the spatial distributions of their electrostatic potentials and to make correlations with the binding properties and pathobiology of FH. These correlations are based on our clustering analysis of electrostatic potentials and knowledge from available experimental and clinical data.

The rationale for our study is that if electrostatics is responsible for binding, we can identify FH CCP modules with similar binding abilities. Besides electrostatic interactions with C3b, FH interacts with negatively charged surfaces because it has binding sites for sialic acid and GAGs, including heparin. Also, if electrostatics plays a known role in disease, through the presence of electrostatic hotspots in the surface of certain CCP modules, then other CCP modules with similar electrostatic profiles may also play a role in the specific disease.

FH is a long and flexible chain-like protein consisting of 20 modules, with each module having distinct properties and role in binding to PBS or C3b/C3c/C3d fragments or other molecules. Also, individual CCP modules have been associated to FH-mediated diseases, such as AMD, aHUS, and DDD. It is reasonable to decompose the binding and pathobiological properties of FH to respective properties of individual CCP modules. Although sequence identities are in the range of 5–40%, a major contributor to the formation of tertiary structures converged to the CCP module topology is the presence of two conserved disulfide bridges. (For clarification, 16 CCP modules have 30–40% identity with one or more CCP modules and 4 have 21–29% identities with one or more CCP modules; Supplementary Table S1.) Our efforts are focused on the role of charge distributions within the tertiary structures and on classifying similarities/dissimilarities of spatial distributions of electrostatic potentials derived from charge. This work provides useful electrostatic analysis to form hypotheses and make predictions for interactions and biological function of FH.

3.2. Clustering of FH modules and C3b domains

Fig. 1 shows the clustering of the spatial distributions of electrostatic potentials for the 20 CCP modules of FH at ionic strengths of 0 mM and 150 mM. The figure depicts which CCP modules have similar electrostatic profile, by taking into account not only charge, but also how the charge-generated electrostatic potential is distributed in space. Although CCP modules with similar charges tend to cluster together, it is the three-dimensional structure of each module and the charge topology within each structure that renders the specific spatial distributions of electrostatic potentials. There are seven CCP modules with positive net charge: CCP1, 5, 7, 10, 13, 17, and 20 (net charges 1–5; Fig. 1). Twelve CCP modules have negative net charge: CCP2, 3, 6, 8, 9, 11, 12, 14, 15, 16, 18, and 19 (net charges −1 to −6; Fig. 1). Only the CCP4 module has 0 net charge (Fig. 1). Because of local cancellation or enhancement of electrostatic potentials in spatial proximity, CCP modules with similar charges may cluster differently, but within the same superclusters (Fig. 1).

At 0 mM counterion concentrations we observe the formation of two superclusters including modules with net charges $Q > 1$ and $Q < -1$, whereas the module with $Q = 0$ forms its own branch on its own within the negative supercluster (Fig. 1A). Finer clustering occurs according to similarities in localized electrostatic properties of modules within each supercluster. At 150 mM counterion concentration we also observe the formation of two superclusters including modules with net charges $Q > 2$ and $Q < -2$. However, modules with net charges 0 and ±1 cluster within the negative supercluster, with 5 out of 6 such modules forming their own cluster (Fig. 1B). This demonstrates the importance of ionic screening of Coulombic interactions, which may reflect on protein function. These data also suggest that spatial distributions of electrostatic potentials may be better predictors for electrostatically driven protein function than net charge alone.

Our analysis focuses on the FH CCP modules, defined with boundaries between the first and fourth conserved cysteines. In addition, the flexible linkers of consecutive CCP modules may mediate electrostatic interactions if they contain charged amino acids. Supplementary Table S2 provides the linker and N- and C-terminal sequences to indicate if they are amenable to electrostatic interactions.

The basic idea behind performing electrostatic potential calculations is that the excess charge in individual CCP modules is responsible for driving FH interactions with target proteins or surfaces. Excess net charge is responsible for non-specific recognition between two proteins or a protein and a ligand carrying opposite net charges, based on long-range electrostatic interactions [25–31,39–41,45,46]. Recognition is followed by specific binding, involving predominantly short-range interactions, such as hydrogen bonds, salt bridges, and hydrophobic. The electrostatic clustering of Fig. 1 presents a quantitative classification of CCP modules with similar electrostatic properties and perhaps similar functions.

3.3. Binding of FH to PBS

Our data suggest that the 5 predominantly positively charged ($Q > 2$) CCP modules are potential interaction sites with polyanions (Fig. 1). CCP modules clustering together may have similar binding properties. These are the CCP1, 5, 7, 13, and 20. An earlier low-resolution structure of FH has proposed a folded-back dynamic structure [21] that may enable multiple modules to recognize the same polyanionic surface. Polyanion-binding sites in CCP19–20 and CCP6–8 have been discussed in the past in view of experimental [48,49] and structural [50,51] data. Also, heparin-binding sites have been previously discussed for CCP7, CCP12–14, and CCP19–20 [48,52]. Fig. 1 suggests that it is impossible for CCP6 to be a polyanion-binding site since it has a net charge of −6. Modules CCP8 and 19 have low probability for binding polyanions since their total charge is −1; however, they both have patches of positive electrostatic potential hotspots, which cannot exclude a localized ability to bind polyanions (Fig. 1). It may also be possible that modules CCP8 and 19 act as scaffolds to orient neighboring modules CCP7 and 20, respectively, for polyanion binding. Previously not discussed, to the best of our knowledge, CCP1 and CCP5 may deserve attention as potential polyanion-binding site, according to Fig. 1.

3.4. Binding of FH to C3b

FH regulates complement activation by interacting with C3b. There are several experimental and structural studies that implicate CCP1–4 and 19–20 and possibly 7 and 12–14 (or 11–15) in binding to C3b [10,14,49,53–56]. CCP19–20 have also been proposed to bind to C3d and CCP12–14 have also been proposed to bind C3c [54], suggesting that different CCP modules may contact different C3b sites. Fig. 2A and B shows the clustering of the spatial distributions of electrostatic potentials for the 8 MG domains of C3b, whose relative topology is shown in Fig. 2C. As is the case with the CCP modules of FH, there is charge diversity in the MG domains of C3b, ranging from excess charge of −6 to excess charge of +8. Fig. 2 depicts two superclusters for positive and negative CCP modules, with finer clustering within each supercluster based on the presence of localized charge hotspots and the inclusion or not of counterions in the calculations. There are other domains in C3b that are not homologous to MG domains and cannot be included in the clustering of Fig. 2. Supplementary Fig. S1 summarizes these domains, their structures and spatial distributions of their electrostatic potentials to indicate possible binding effects. The overall electrostatic potential of C3b is excessively negative (Fig. 2D), with profound contributions from non-MG domains, such as a'Nt, C3d, CUB, LNK, and C345 C with net charges −5, −4, −6, +2, and −12, respectively (Supplementary Fig. S1). Only 3 MG domains and LNK have positive net charges. Taking into account the dynamics of C3b,

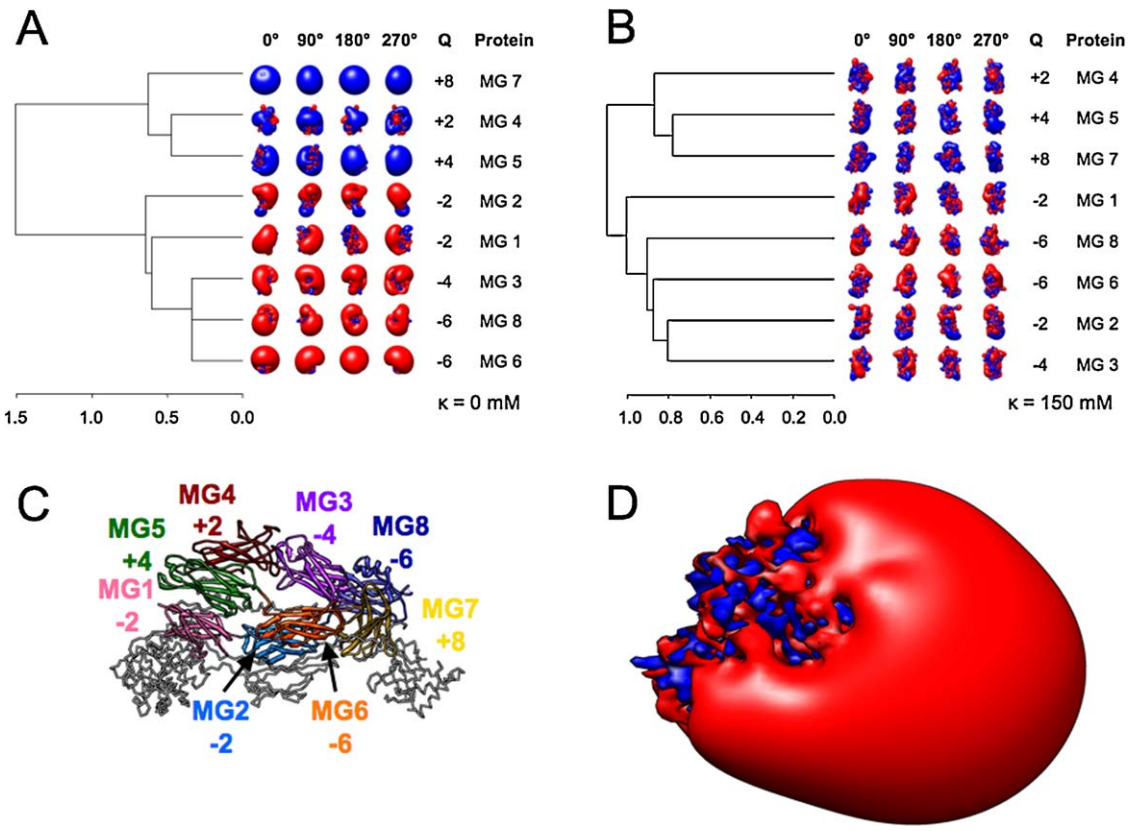

Fig. 2. Clustering diagram of the 8 MG domains of C3b (PDB Code 2I07) according to the spatial distributions of their electrostatic potentials. Calculations of electrostatic potentials were performed using ionic strengths corresponding to 0 mM (A) and 150 mM (B) counterion concentration. Isopotential contours are plotted at $\pm 1 k_B T/e$, with blue and red corresponding to positive and negative electrostatic potential, respectively. Four orientations are shown corresponding to rotations about the vertical axis, as indicated. The net charge, *Q*, of each module is marked in the figure. (C) The 8 MG domains are shown in ribbon representations with different colors, as marked. The net charge of each MG domain is also marked. The amino acid ranges for each of the C3b domains are: MG1 (1–104), MG2 (105–209), MG3 (210–328), MG4 (329–426), MG5 (427–534), MG6 (535–577 and 746-806), MG7 (807-911), MG8 (1331–1474). (D) Isopotential contour plot for C3b at $\pm 3 k_B T/e$. The color code is blue for positive and red for negative electrostatic potential. The calculation of electrostatic potential was performed using ionic strength corresponding to 0 mM counterion concentration. (For interpretation of the references to color in this figure legend, the reader is referred to the web version of the article.)

it is likely that there are transient openings that expose positively charged patches in C3b which may be sites of interaction with negatively charged CCP modules of FH.

When we initiated this study, we expected, to a large extent, complementary electrostatic properties for interacting macrodipoles between C3b domains and FH modules. Although we recognize that the tertiary structure of C3b, which is rather compact, may introduce cancellations or enhancements in the electrostatic potentials at the vicinities of neighboring domains that contact each other, this may not be the case for FH whose modules form an extended chain-like structure. When the crystallographic structure of the complex between FH(CCP1–4) and C3b was published [22], the following contacts were observed: (i) positive–negative net charge, CCP1–α′Nt and Linker(CCP1–CCP2)–α′Nt; neutral–negative net charge, CCP4–C3d and CCP4–MG1; positive–positive net charge, CCP1–MG7 and Linker(CCP1–CCP2)–α′Nt; negative–negative net charge, CCP2–α′Nt, CCP2–MG2, CCP2–MG6, CCP3–CUB, CCP3–MG1, and CCP3–MG2 (Fig. 3). The types of contacts, decomposed to hydrogen bond and salt bridge (up to 3.5 Å), Coulombic (up to 8 Å), and hydrophobic interactions, are summarized in Supplementary Tables S3, S4, and S5. In all cases, there are strong local pairwise interactions that stabilize the interacting FH(module)–C3b(domain) complexes. All interacting module–domain complexes involve at least one salt bridge and many hydrogen bonding, and Coulombic interactions. Hydrophobic interactions are more prominent in the case of CCP1 and 2 compared to CCP3 and 4. Fig. 3B and C shows a surface projection of the electrostatic potential complementarity for the FH(CCP1–4)–C3b complex, depicting interacting positive–negative hotspots or positive/negative–neutral areas.

Based on our findings and guided by the crystal structure, we propose the following model for FH(CCP1–4)–C3b recognition and binding. The recognition process is driven by long-range interactions between the positive CCP1/Linker(CCP1–CCP2) and the negative α′Nt, which orient FH on the surface of C3b to favor specific short-range interactions and lock binding. Upon formation of the non-specific encounter complex, local structural rearrangements and solvent exclusion take place to accommodate favorable short-range interactions for binding. The binding step is dominated by the stronger and specific pairwise interactions in local areas of complementary charge hotspots or neutral-charged spots. In our analysis, above, long-range electrostatic interactions are depicted by the spatial distributions of electrostatic potentials and short-range electrostatic interactions are depicted by the surface projections of electrostatic potentials. Our analysis shows that charge distributions and electrostatic potential distributions are more useful in understanding C3b–FH interactions than net charges alone. Our clustering analysis shows stronger ionic strength effect on neutral or slightly charged (+/−1) modules/domains. The 0 mM clustering data of excessively charged modules/domains ($|Q| \geq 2$), although non-physiological, contain less localized electrostatic hotspots, as would be expected by the inclusion of the dynamic character of amino acid side chains.

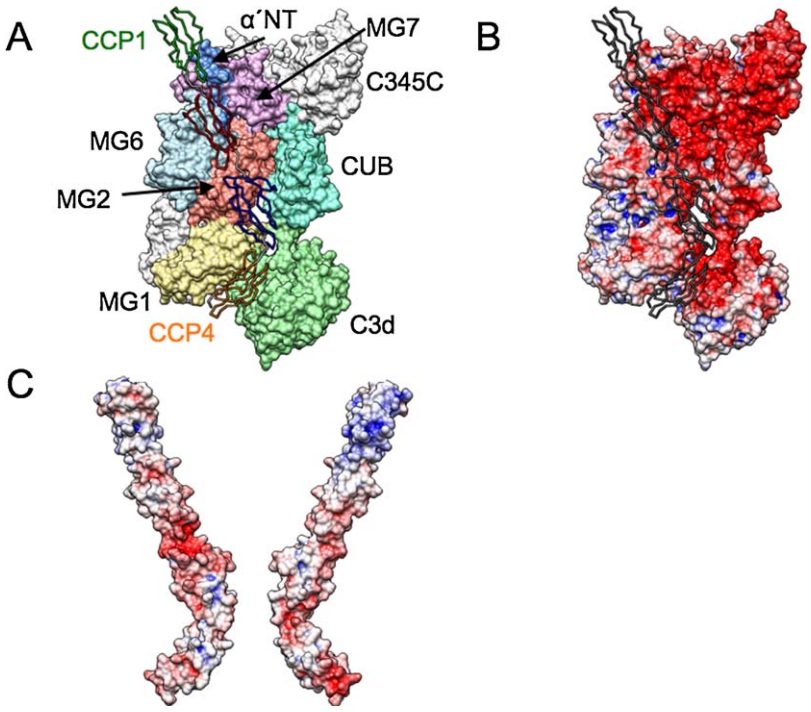

Fig. 3. (A) FH(CCP1–4) in C^{α}-trace representation and C3b in a surface representation. The 8 MG domains and the C3d, C345C, CUB, and α'Nt domains are shown in different colors and marked. CCP1 and CCP2 of FH are also marked. (B) FH(CCP1–4) in C^{α}-trace representation and C3b in surface representation, colored by projection of its electrostatic potential. (C) FH(CCP1–4) in surface representation, colored by projection of its electrostatic potential. The right image of (C) is the contact surface of FH(CCP1–2) with C3b in the orientation of panel (B) and. Comparison of panels (B) and (C) depicts electrostatic potential complementarity. The color code in (B) and (C) is blue for positive and red for negative electrostatic potential. (For interpretation of the references to color in this figure legend, the reader is referred to the web version of the article.)

3.5. Pathobiology of FH

Previous studies have shown that the FH module CCP7 is involved in AMD through the Tyr/His402 SNP, with His being the amino acid of the population at risk [4,6–8]. We have performed pK_a calculations to investigate if Tyr402 (an acidic amino acid with model pK_a of 9.6) or His402 (a basic amino acid with model pK_a of 6.3) are found in conformationally strained environments. This would have been indicated by unusual shifts in pK_a values; however this was not the case (data not shown). Indeed both Tyr402 and His402 are solvent exposed in the NMR structures [57], which suggests freedom of the amino acid in position 402 for involvement in specific side chain intermolecular interactions possibly with C3b. CCP7 has also a polyanion-binding hotspot on its surface [14] and overall positive electrostatic potential (Fig. 1), which may be important for nonspecific interactions with negatively charged regions of C3b. Barlow and coworkers discuss the possibility of disruption of the ability of FH to bind GAGs upon mutation of Tyr402 to His402 [57]. They propose that the interaction of CCP7 with heparin or sulfated heparin oligosaccharides is driven by ring stacking interactions of the two tyrosine-rich regions of CCP7 (Tyr390, Tyr393, Tyr402 and 398, Tyr420) and sugar rings. This interaction may be perturbed upon removal of Tyr402 and replacement by His402 in the genetically predisposed population for AMD. A unit charge of the SNP amino acid, does not appear to play a role, as both Tyr402 and His402 are expected to be neutral at physiological pH since they are solvent exposed and our calculations do not suggest pK_a perturbations. In essence, the model of Barlow and coworkers [57] implicates ring stacking in addition to overall charge complementarity in the case of heparin and GAGs in general. The same study provides a structural picture of these interactions using chemical shift perturbation mapping of NMR data and suggests the presence of two faces of interaction. Another study also suggests differential heparin binding for the Tyr402 and His402 variants of CCP6–8 [58]. Finally, the crystal structures of CCP6–8(His402) (with the genetic variation His402) in complex with sucrose octasulfate demonstrates proximity of Tyr390 and His402 with sulfate groups [51].

Module CCP4 is involved in DDD through deletion of Lys224 [19]. CCP4 is the only neutral module of FH, with balanced, and rather unusual, spatial distribution of electrostatic potential (Fig. 1). According the FH(CCP1–4)–C3b crystal structure, CCP4 contacts the negatively charged domains C3d and MG1. It is likely that the deletion of the positively charged Lys224 produces an imbalance in the spatial distribution of electrostatic potential of CCP4. This would favor excess negative electrostatic potential which may be disruptive for the binding of CCP4. It is possible that module CCP7 is also involved in DDD through the polyanion-binding hotspot [14]. Interestingly, there is a link between DDD and AMD because often patients have both diseases [59].

Modules CCP19–20 are involved in aHUS, because many aHUS-associated mutations are located in CCP20 [10,14,17,48,49,60,61]. Our data suggest that CCP20 is a polyanion-binding site because of its excess positive spatial distribution of electrostatic potential (Fig. 1). On the contrary, CCP19, with net charge −1, has a somehow balanced spatial distribution of electrostatic potential (Fig. 1). The role of CCP19 may be that of a scaffold to properly orient the structure of CCP20 or binding to C3b/C3d; however, a recent study suggests that CCP19 may also be a binding module to C3b/C3d [62], which may be possible through localized short-range interactions. It is likely that the observed mutations in CCP19–20 affect both functions of these modules, their polyanion-binding ability and their ability to bind C3b/C3d. A number of C3b mutations have also been reported to be associated with aHUS, however these mutations are enhancing or inhibiting mainly the interaction of C3b with membrane cofactor protein (MCP) [63]. Some of these mutations involve ionizable amino acids. Additional studies to identify similar mutations that affect C3b/C3d interactions with FH are necessary.

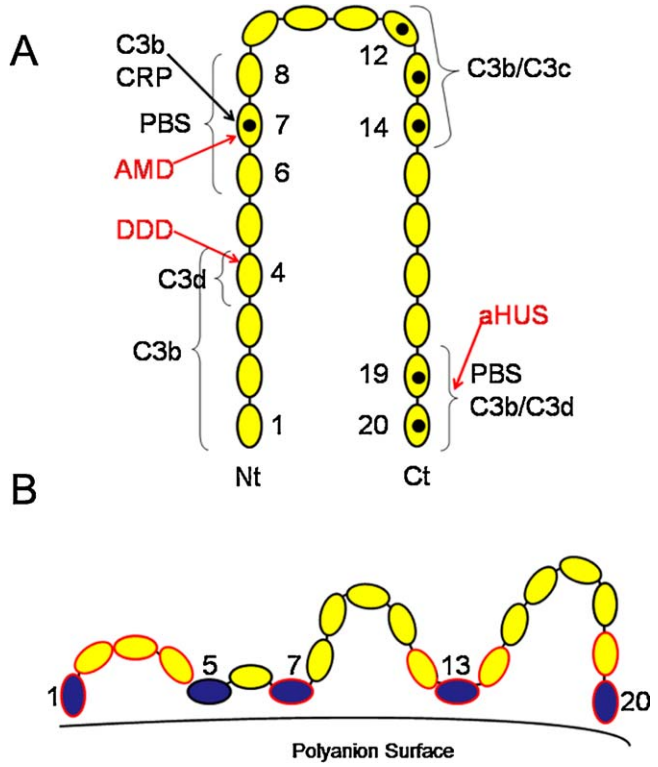

Fig. 4. Cartoon representing our model for FH interactions with polyanion-containing surfaces and C3b. Other interaction sites are also marked. The CCP modules or module ranges discussed in text are numbered. (A) A simple model based on previous structural and mutagenesis data, which implicate CCP20 in anchoring polyanion-rich surfaces and CCP1–4, CCP7, 12–14 and 19–20 in interacting with C3b and its fragments. CCP modules that contain previously proposed polyanion-binding sites (PBS) are marked. The N- and C-termini are marked. The black dots indicate heparin binding sites. The CCP7 module interacting with C-reactive protein (CRP) is marked. CCP modules implicated in complement-mediated disease, such as AMD, DDD, and aHUS are marked in red. (B) A more elaborate model that incorporates electrostatic properties from our analysis. This model implicates CCP1, CCP5, CCP7, CCP13, and CCP20 in interactions with polyanion-rich sites. CCP modules colored in blue possess polyanion-binding sites and those with red borders are C3b-binding sites, in analogy with panel (A). (For interpretation of the references to color in this figure legend, the reader is referred to the web version of the article.)

3.6. Model for FH interactions with PBS and C3d

Fig. 4A presents a previously published functional map of FH [56], including an additional C3d binding site for CCP4, identified by the crystal structure of FH(CCP1–4)–C3b (PDB Code: 2WII) [22]. These interactions are hypothesized to be responsible for regulation of the complement system in self-surfaces. The presence of a complex bending of FH is likely, to allow contact of the polyanion-binding site of CCP6–8 with cell surfaces; however, according to our data, only the highly positively charged CCP7 of this triplet is capable of binding to polyanion sites. We propose a modified model which includes anchoring of FH on cell surfaces through polyanion-binding sites in the 5 excessively positively charged modules CCP1, 5, 7, 13 and 20. This binding allows for the following sets of interactions with C3b/C3d: (i) CCP1–4, 7, 12–14, and 19–20 with C3b; and (ii) CCP4 and 19–20 with the C3d portion of C3b. As C3d is the opsonization site, it must be in proximity to the cell surfaces, and so can be the positively charged modules CCP1, 5, 7, 13, and 20. This can happen in a 1:1 complex, which would bring CCP4 and 19–20 in a topology surrounding C3d, or in bivalent complexes. Recent studies have suggested that FH undergoes self-association in the presence of polyanions [60,62,64,65]. It is likely that the function of FH and implication to disease is more complex than presented here. However, the presented electrostatic arguments for association with polyanions and disease-related mutations are applicable for monomers and also for higher order self-associated complexes.

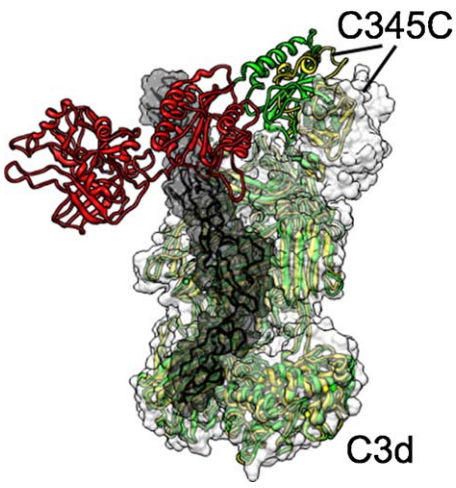

Fig. 5. Competition in the formation of C3b complexes. Superposition of the C3b–FH(CCP1–4) and C3b–Bb (C3 convertase) complexes and free C3b. The structure of the C3b–FH complex (C3b in white, FH in black) is shown in surface representation, while the C3b–Bb complex is shown in ribbon representation (C3b in green, Bb in red) and free C3b is shown in yellow ribbon representation. Conformational transitions involving mainly the C345C domain of C3b are identifiable in the figure. The PDB Codes are 2WII for C3b–FH(CCP1–4), 2WIN for C3b–Bb, and 2I07 for free C3b.

Our model proposes non-specific electrostatic interactions with polyanion surfaces and specific electrostatic (and non-electrostatic) interactions with C3b. Non-specific interactions with polyanions in self surfaces result in high concentration of FH molecules, which become available for C3b binding and subsequent C3b degradation. The number of C3b molecules is sparse in self-surfaces because of lack of (or reduced) amplification loop of the complement system alternative pathway. On the contrary, in non-self surfaces there is less concentration of FH molecules and excess of the C3 convertase C3b–Bb. The latter is responsible for the amplification of C3 cleavage, which generates numerous copies of the C3b opsonin for pathogen surface coating, and subsequent elimination by phagocytosis. We can also factor in this model possible auto-inhibitory association interactions between positive and negative CCP modules (or hotspots). This type auto-association may be present in free FH, which, in the presence of PBS, unwinds to accommodate binding to C3b.

Barlow and coworkers have previously presented a binding model involving anchoring of CCP20 to self-surface through "C3b/polyanion composite binding site", with CCP7 acting as a mediator and CCP1–4 disrupting the formation and stability of C3/C5 convertases [56]. The proposed mediating ability of CCP7 was called "proof-reading" to aid discrimination of self from non-self sulfation patterns [56]. The choice of the intermediate module CCP7 as the mediator may be based on the fact that it is part of the binding site of many bacteria known to interact with FH [9,20,48]; however, there are bacterial binding sites that do not include CCP7 [48]. The hypothesis of Barlow and coworkers is attractive and overall in line with our electrostatic data.

A fundamental question rises on the physicochemical basis of the competition between FH and the C3 convertase C3b–Bb for C3b binding on self and non-self surfaces. Fig. 5 shows a superposition of the C3b–FH(CCP1–4) and C3b–Bb complexes, which demonstrates how FH(CCP1–4) binding can sterically hinder C3b–Bb access to its binding site [22]. According to our model FH(CCP1–4) binding is facilitated by non-specific electrostatic interactions between positive CCP modules and polyanion sites in self surfaces. FH(CCP1–4) binding is initiated by the electrostatic recognition of

CCP1 and α′Nt. Upon FH binding, a conformational transition is observed in C3b involving moving away of the negatively charged C345C domain ($Q = -12$) (Fig. 5), possibly owed to non-specific electrostatic repulsion with CCP2 ($Q = -6$) and CCP3 ($Q = -4$). Conformational transition in the opposite direction occurs upon Bb binding to C3b involving the C345C domain (Fig. 5). In summary, it is likely that synergistic binding of the positive FH CCP modules to polyanion surfaces and specific C3b–FH contacts contribute to the formation of a stronger C3b–FH complex than a C3b–Bb complex on self surfaces.

Although most of the binding studies are based on experimental mutagenesis studies or CCP module deletions, our electrostatic and clustering analysis together with structural data provide additional tools to guide future experiments that are needed for refining the proposed model of C3b–FH interaction. The electrostatic data are useful to establish mechanistic hypotheses for C3b–FH and C3b–Bb interactions.

Acknowledgement

C.A.K. would like to acknowledge the TRDRP Dissertation Fellowship for financial support.

Appendix A. Supplementary data

Supplementary data associated with this article can be found, in the online version, at doi:10.1016/j.jmgm.2011.04.010.

References

[1] V.P. Ferreira, M.K. Pangburn, C. Cortes, Complement control protein factor H: the good, the bad, and the inadequate, Mol. Immunol. 47 (2010) 2187–2197.
[2] M.J. Walport, Advances in immunology: complement (first of two parts), N. Engl. J. Med. 344 (2001) 1058–1066.
[3] M.J. Walport, Advances in immunology: complement (second of two parts), N. Engl. J. Med. 344 (2001) 1140–1144.
[4] A.O. Edwards, R. Ritter, K.J. Abel, A. Manning, C. Panhuysen, L.A. Farrer, Complement factor H polymorphism and age-related macular degeneration, Science 308 (2005) 421–424.
[5] K.M. Gehrs, D.H. Anderson, L.V. Johnson, G.S. Hageman, Age-related macular degeneration – emerging pathogenetic and therapeutic concepts, Ann. Med. 38 (2006) 450–471.
[6] G.S. Hageman, D.H. Anderson, L.V. Johnson, L.S. Hancox, A.J. Taiber, L.I. Hardisty, J.L. Hageman, H.A. Stockman, J.D. Borchardt, K.M. Gehrs, R.J.H. Smith, G. Silvestri, S.R. Russell, C.C.W. Klaver, I. Barbazetto, S. Chang, L.A. Yannuzzi, G.R. Barile, J.C. Merriam, R.T. Smith, A.K. Olsh, J. Bergeron, J. Zernant, J.E. Merriam, B. Gold, M. Dean, R. Allikmets, A common haplotype in the complement regulatory gene factor H (HF1/CFH) predisposes individuals to age-related macular degeneration, Proc. Natl. Acad. Sci. U.S.A. 102 (2005) 7227–7232.
[7] J.L. Haines, M.A. Hauser, S. Schmidt, W.K. Scott, L.M. Olson, P. Gallins, K.L. Spencer, S.Y. Kwan, M. Noureddine, J.R. Gilbert, N. Schnetz-Boutaud, A. Agarwal, E.A. Postel, M.A. Pericak-Vance, Complement factor H variant increases the risk of age-related macular degeneration, Science 308 (2005) 419–421.
[8] R.J. Klein, C. Zeiss, E.Y. Chew, J.Y. Tsai, R.S. Sackler, C. Haynes, A.K. Henning, J.P. SanGiovanni, S.M. Mane, S.T. Mayne, M.B. Bracken, F.L. Ferris, J. Ott, C. Barnstable, J. Hoh, Complement factor H polymorphism in age-related macular degeneration, Science 308 (2005) 385–389.
[9] J.P. Atkinson, T.H.J. Goodship, Complement factor H and the hemolytic uremic syndrome, J. Exp. Med. 204 (2007) 1245–1248.
[10] J. Caprioli, M. Noris, S. Brioschi, G. Pianetti, F. Castelletti, P. Bettinaglio, C. Mele, E. Bresin, L. Cassis, S. Gamba, F. Porrati, S. Bucchioni, G. Monteferrante, C.J. Fang, M.K. Liszewski, D. Kavanagh, J.P. Atkinson, G. Remuzzi, Genetics of HUS: the impact of MCP, CFH, and IF mutations on clinical presentation, response to treatment, and outcome, Blood 108 (2006) 1267–1279.
[11] S.R de Cordoba, E.G. de Jorge, Translational mini-review series on complement factor H: genetics and disease associations of human complement factor H, Clin. Exp. Immunol. 151 (2008) 1–13.
[12] C.J. Fang, A. Richards, M.K. Liszewski, D. Kavanagh, J.P. Atkinson, Advances in understanding of pathogenesis of aHUS and HELLP, Brit. J. Haematol. 143 (2008) 336–348.
[13] G.B. Appel, H.T. Cook, G. Hageman, J.C. Jennette, M. Kashgarian, M. Kirschfink, J.D. Lambris, L. Lanning, H.U. Lutz, S. Meri, N.R. Rose, D.J. Salant, S. Sethi, R.J.H. Smith, W. Smoyer, H.F. Tully, S.P. Tully, P. Walker, M. Welsh, R. Wurzner, P.F. Zipfel, Membranoproliferative glomerulonephritis type II (dense deposit disease): an update, J. Am. Soc. Nephrol. 16 (2005) 1392–1403.
[14] P. Gros, F.J. Milder, B.J.C. Janssen, Complement driven by conformational changes, Nat. Rev. Immunol. 8 (2008) 48–58.
[15] B.J.C. Janssen, P. Gros, Structural insights into the central complement component C3, Mol. Immunol. 44 (2007) 3–10.
[16] D. Serruto, R. Rappuoli, M. Scarselli, P. Gros, J.A.G. van Strijp, Molecular mechanisms of complement evasion: learning from staphylococci and meningococci, Nat. Rev. Microbiol. 8 (2010) 393–399.
[17] R.E. Saunders, C.A. Garrido, V. Fremeaux-Bacchi, E.G. de Jorge, T.H.J. Goodship, M.L. Trascasa, M. Noris, I.M.P. Castro, G. Remuzzi, S.R. de Cordoba, P.S. Corral, C. Skerka, P.F. Zipfel, S.J. Perkins, The interactive factor H-atyplical hemolytic uremic syndrome mutation database and website: update and integration of membrane cofactor protein and factor I mutations with structural models, Hum. Mutat. 28 (2007) 222–234.
[18] C.Q. Schmidt, A.P. Herbert, H.G. Hocking, D. Uhrin, P.N. Barlow, Translational mini-review series on complement factor H: structural and functional correlations for factor H, Clin. Exp. Immunol. 151 (2008) 14–24.
[19] C. Licht, S. Heinen, M. Jozsi, I. Loschmann, R.E. Saunders, S.J. Perkins, R. Waldherr, C. Skerka, M. Kirschfink, B. Hoppe, P.F. Zipfel, Deletion of Lys224 in regulatory domain 4 of factor H reveals a novel pathomechanism for dense deposit disease (MPGN II), Kidney Int. 70 (2006) 42–50.
[20] D.C. Soares, P.N. Barlow, Complement control protein modules in the regulators of complement activation, in: D. Morikis, J.D. Lambris (Eds.), In Structural Biology of the Complement System, Taylor & Francis/CRC Press, Boca Raton, Florida, 2005, 19 62.
[21] M. Aslam, S.J. Perkins, Folded-back solution structure of monomeric factor H of human complement by synchrotron X-ray and neutron scattering, analytical ultracentrifugation and constrained molecular modeling, J. Mol. Biol. 309 (2001) 1117–1138.
[22] J. Wu, Y.Q. Wu, D. Ricklin, B.J.C. Janssen, J.D. Lambris, P. Gros, Structure of complement fragment C3b–factor H and implications for host protection by complement regulators, Nat. Immunol. 10 (2009) 728–734.
[23] B.J.C. Janssen, A. Christodoulidou, A. McCarthy, J.D. Lambris, P. Gros, Structure of C3b reveals conformational changes that underlie complement activity, Nature 444 (2006) 213–216.
[24] N.A. Baker, D. Sept, S. Joseph, M.J. Holst, J.A. McCammon, Electrostatics of nanosystems: application to microtubules and the ribosome, Proc. Natl. Acad. Sci. U.S.A. 98 (2001) 10037–10041.
[25] A. Cheung, C.A. Kieslich, J. Yang, D. Morikis, Solvation effects in calculated electrostatic association free energies for the C3d–CR2 complex, and comparison to experimental data, Biopolymers 93 (2010) 509–519.
[26] D Morikis, J.D. Lambris, The electrostatic nature of C3d-complement receptor 2 association, J. Immunol. 172 (2004) 7537–7547.
[27] D. Morikis, L. Zhang, An immunophysical study of the complement system: examples for the pH dependence of protein binding and stability, J. Non-Cryst. Solids 352 (2006) 4445–4450.
[28] K. Pyaram, C.A. Kieslich, V.N. Yadav, D. Morikis, A. Sahu, Influence of electrostatics on the complement regulatory functions of kaposica, the complement inhibitor of Kaposi's sarcoma-associated herpesvirus, J. Immunol. 184 (2010) 1956–1967.
[29] G. Sfyroera, M. Katragadda, D. Morikis, S.N. Isaacs, J.D. Lambris, Electrostatic modeling predicts the activities of orthopoxvirus complement control proteins, J. Immunol. 174 (2005) 2143–2151.
[30] L. Zhang, B. Mallik, D. Morikis, Immunophysical exploration of C3d–CR2(CCP1–2) interaction using molecular dynamics and electrostatics, J. Mol. Biol. 369 (2007) 567–583.
[31] L. Zhang, D. Morikis, Immunophysical properties and prediction of activities for vaccinia virus complement control protein and smallpox inhibitor of complement enzymes using molecular dynamics and electrostatics, Biophys. J. 90 (2006) 3106–3119.
[32] J. Schultz, F. Milpetz, P. Bork, C.P. Ponting, SMART, a simple modular architecture research tool: identification of signaling domains, Proc. Natl. Acad. Sci. U.S.A. 95 (1998) 5857–5864.
[33] M.A. Larkin, G. Blackshields, N.P. Brown, R. Chenna, P.A. McGettigan, H. McWilliam, F. Valentin, I.M. Wallace, A. Wilm, R. Lopez, J.D. Thompson, T.J. Gibson, D.G. Higgins, Clustal W and clustal X version 2.0, Bioinformatics 23 (2007) 2947–2948.
[34] M.A. Marti-Renom, A.C. Stuart, A. Fiser, R. Sanchez, F. Melo, A. Sali, Comparative protein structure modeling of genes and genomes, Annu. Rev. Biophys. Biomol. Struct. 29 (2000) 291–325.
[35] N. Guex, M.C. Peitsch, SWISS-MODEL and the Swiss-PdbViewer: an environment for comparative protein modeling, Electrophoresis 18 (1997) 2714–2723.
[36] T.J. Dolinsky, J.E. Nielsen, J.A. McCammon, N.A. Baker, PDB2PQR: an automated pipeline for the setup of Poisson–Boltzmann electrostatics calculations, Nucleic Acids Res. 32 (2004) W665–W667.
[37] D. Sitkoff, K.A. Sharp, B. Honig, Accurate calculation of hydration free energies using macroscopic solvent models, J. Phys. Chem. 98 (1994) 1978–1988.
[38] E.F. Pettersen, T.D. Goddard, C.C. Huang, G.S. Couch, D.M. Greenblatt, E.C. Meng, T.E. Ferrin, UCSF chimera – a visualization system for exploratory research and analysis, J. Comp. Chem. 25 (2004) 1605–1612.
[39] N. Blomberg, R.R. Gabdoulline, M. Nilges, R.C. Wade, Classification of protein sequences by homology modeling and quantitative analysis of electrostatic similarity, Proteins 37 (1999) 379–387.
[40] C.A. Kieslich, R.D. Gorham, D. Morikis, Is the rigid-body assumption reasonable? Insights into the effects of dynamics on the electrostatic analysis of barnase–barstar, J. Non-Cryst. Solids 357 (2011) 707–716.

[41] C.A. Kieslich, D. Morikis, J. Yang, D. Gunopulos, Automated computational framework for the analysis of electrostatic similarities of proteins, Biotechnol. Prog. 27 (2011) 316–325.
[42] J.D. Petke, Cumulative and discrete similarity analysis of electrostatic potentials and fields, J. Comp. Chem. 14 (1993) 928–933.
[43] K. Schleinkofer, U. Wiedemann, L. Otte, T. Wang, G. Krause, H. Oschkinat, R.C. Wade, Comparative structural and energetic analysis of WW domain–peptide interactions, J. Mol. Biol. 344 (2004) 865–881.
[44] M. Stein, R.R. Gabdoulline, R.C. Wade, Cross-species analysis of the glycolytic pathway by comparison of molecular interactions fields, Mol. Biosyst. 6 (2010) 162–174.
[45] R.C. Wade, R.R. Gabdoulline, S.K. Ludemann, V. Lounnas, Electrostatic steering and ionic tethering in enzyme–ligand binding: insights from simulations, Proc. Natl. Acad. Sci. U.S.A. 95 (1998) 5942–5949.
[46] X.Y. Zhang, C.L. Bajaj, B. Kwon, T.J. Dolinsky, J.E. Nielsen, N.A. Baker, Application of new multiresolution methods for the comparison of biomolecular electrostatic properties in the absence of global structural similarity, Multiscale Model. Sim. 5 (2006) 1196–1213.
[47] R Development Core Team, R: A language and environment for statistical computing. R Foundation for Statistical Computing: Vienna, Austria, 2009. http://www.R-project.org.
[48] S.R. de Cordoba, J. Esparza-Gordillo, E.G. de Jorge, M. Lopez-Trascasa, P. Sanchez-Corral, The human complement factor H: functional roles, genetic variations and disease associations, Mol. Immunol. 41 (2004) 355–367.
[49] V.P. Ferreira, A.P. Herbert, H.G. Hocking, P.N. Barlow, M.K. Pangburn, Critical role of the C-terminal domains of factor H in regulating complement activation at cell surfaces, J. Immunol. 177 (2006) 6308–6316.
[50] A.P. Herbert, D. Uhrin, M. Lyon, M.K. Pangburn, P.N. Barlow, Disease-associated sequence variations congregate in a polyanion recognition patch on human factor H revealed in three-dimensional structure, J. Biol. Chem. 281 (2006) 16512–16520.
[51] B.E. Prosser, S. Johnson, P. Roversi, A.P. Herbert, B.S. Blaum, J. Tyrrell, T.A. Jowitt, S.J. Clark, E. Tarelli, D. Uhrin, P.N. Barlow, R.B. Sim, A.J. Day, S.M. Lea, Structural basis for complement factor H-linked age-related macular degeneration, J. Exp. Med. 204 (2007) 2277–2283.
[52] T.K. Blackmore, J. Hellwage, T.A. Sadlon, N. Higgs, P.F. Zipfel, H.M. Ward, D.L. Gordon, Identification of the second heparin-binding domain in human complement factor H, J. Immunol. 160 (1998) 3342–3348.
[53] G.J. Arlaud, P.N. Barlow, C. Gaboriaud, P. Gros, S.V.L. Narayana, Deciphering complement mechanisms: the contributions of structural biology, Mol. Immunol. 44 (2007) 3809–3822.
[54] T.S. Jokiranta, J. Hellwage, V. Koistinen, P.F. Zipfel, S. Meri, Each of the three binding sites on complement factor H interacts with a distinct site on C3b, J. Biol. Chem. 275 (2000) 27657–27662.
[55] C.Q. Schmidt, A.P. Herbert, D. Kavanagh, C. Gandy, C.J. Fenton, B.S. Blaum, M. Lyon, D. Uhrin, P.N. Barlow, A new map of glycosaminoglycan and C3b binding sites on factor H, J. Immunol. 181 (2008) 2610–2619.
[56] A.K. Sharma, M.K. Pangburn, Identification of three physically and functionally distinct binding sites for C3b in human complement factor H by deletion mutagenesis, Proc. Natl. Acad. Sci. U.S.A. 93 (1996) 10996–11001.
[57] A.P. Herbert, J.A. Deakin, C.Q. Schmidt, B.S. Blaum, C. Egan, V.P. Ferreira, M.K. Pangburn, M. Lyon, D. Uhrin, P.N. Barlow, Structure shows that a glycosaminoglycan and protein recognition site in factor H is perturbed by age-related macular degeneration-linked single nucleotide polymorphism, J. Biol. Chem. 282 (2007) 18960–18968.
[58] S.J. Clark, V.A. Higman, B. Mulloy, S.J. Perkins, S.M. Lea, R.B. Sim, A.J. Day, His-384 allotypic variant of factor H associated with age-related macular degeneration has different heparin binding properties from the non-disease-associated form, J. Biol. Chem. 281 (2006) 24713–24720.
[59] R.F. Mullins, N. Aptsiauri, G.S. Hageman, Structure and composition of drusen associated with glomerulonephritis: implications for the role of complement activation in drusen biogenesis, Eye 15 (2001) 390–395.
[60] T.S. Jokiranta, V.P. Jaakola, M.J. Lehtinen, M. Parepalo, S. Meri, A. Goldman, Structure of complement factor H carboxyl-terminus reveals molecular basis of atypical haemolytic uremic syndrome, EMBO J. 25 (2006) 1784–1794.
[61] A. Richards, M.R. Buddles, R.L. Donne, B.S. Kaplan, E. Kirk, M.C. Venning, C.L. Tielemans, J.A. Goodship, T.H.J. Goodship, Factor H mutations in hemolytic uremic syndrome cluster in exons 18–20, a domain important for host cell recognition, Am. J. Hum. Genet. 68 (2001) 485–490.
[62] A. Bhattacharjeea, M.J. Lehtinen, T. Kajanderb, A. Goldmanb, T.S. Jokiranta, Both domain 19 and domain 20 of factor H are involved in binding to complement C3b and C3d, Mol. Immunol. 47 (2010) 1686–1691.
[63] V. Fremeaux-Bacchi, E.C. Miller, M.K. Liszewski, L. Strain, J. Blouin, A.L. Brown, N. Moghal, B.S. Kaplan, R.A. Weiss, K. Lhotta, G. Kapur, T. Mattoo, H. Nivet, W. Wong, S. Gie, B.H. de Ligny, M. Fischbach, R. Gupta, R. Hauhart, V. Meunier, C. Loirat, M.A. Dragon-Durey, W.H. Fridman, B.J.C. Janssen, T.H.J. Goodship, J.P. Atkinson, Mutations in complement C3 predispose to development of atypical hemolytic uremic syndrome, Blood 112 (2008) 4948–4952.
[64] A.I. Okemefuna, K. Li, R. Nan, R.J. Ormsby, T. Sadlon, D.L. Gordon, S.J. Perkins, Multimeric interactions between complement factor H and its C3d ligand provide new insight on complement regulation, J. Mol. Biol. 391 (2009) 119–135.
[65] M.K. Pangburn, N. Rawal, C. Cortes, M.N. Alam, V.P. Ferreira, M.A.L. Atkinson, Polyanion-induced self-association of complement factor H, J. Immunol. 182 (2009) 1061–1068.